JOURNAL OF GUIDANCE, CONTROL, AND DYNAMICS
Vol. 20, No. 5, September–October 1997

Improved Eigenstructure Assignment Controller Design Using a Substructure-Based Coordinate System

Michael J. Triller* and Daniel C. Kammer†
University of Wisconsin, Madison, Wisconsin 53706

A new control coordinate system based on the Craig–Bampton substructure representation is examined for reduced-order-model-based controller design. Eigenstructure assignment controller design using the proposed modeling approach is shown to exhibit improved accuracy over conventional normal mode modeling in both closed-loop eigenvalue and eigenvector attainment. The improvement is due to the coordinate system's ability to accurately predict actuator boundary conditions and, thus, actuator command forces, when extensive model reduction has been employed. Two multi-input/multi-output design examples are used to illustrate the practicality of the method and the resulting improved closed-loop behavior.

Introduction

AEROSPACE vehicles are extremely large flexible structures requiring very accurate shape and vibration control to meet performance objectives. The presence of very low-frequency structural dynamics and dense packing of very lightly damped modes in such systems may lead to a strong interaction between the structure and its control system. These vehicles are infinite dimensional distributed parameter systems, which are usually modeled by the finite element method as a set of ordinary differential equations. This results in a lumped parameter system of finite dimension. Although finite in dimension, these models often contain thousands or even hundreds of thousands of degrees of freedom (DOF) and require extensive model reduction to be practical for structural and control design and simulation.

Recent literature has investigated the use of a new control coordinate system based on the Craig–Bampton (CB) substructure representation.[1–4] The CB coordinate system is the most common representation for loads analysis used in the aerospace industry today.[5] Large CB finite element models (FEM) may be reduced to accurate design and simulation models by truncating dynamically unimportant fixed interface modes using the effective interface mass (EIM) measure of controllability/observability.[6] This measure has been shown to preserve controller/structure interaction in the reduced-order models (ROM) providing accurate closed-loop control designs.

This paper specifically addresses the advantages of reduced CB-based control coordinate systems in closed-loop modern control design applications over reduced normal mode representations. In particular, eigenstructure assignment[7,8] algorithms (ESA) applied to the natural second-order form of the CB equations of motion are shown to lead to more accurate attainment of the desired closed-loop eigenstructure. Two examples are presented to illustrate the improved ESA controller designs obtained. The CB designs are shown to produce smaller gain norms, reflecting more accurate prediction of actuation commands by the reduced-order model. Closed-loop improvements are found in both the closed-loop eigenvalues and right and left eigenvectors. Eigenvector shaping in complex systems has typically been directed at producing robust minimum norm gain solutions in the control design process. The ability to shape eigenvector elements in a simple and highly accurate manner, as presented here, may offer additional flexibility in the selection of the closed-loop elements for highly complex systems without compromising stability in the designs implementation.

Received Nov. 16, 1996; revision received April 15, 1997; accepted for publication April 28, 1997.

*Graduate Research Assistant, Department of Engineering Mechanics and Astronautics; currently Staff Engineer, TRW Space and Electronics Group, Redondo Beach, CA 90278. Member AIAA.

†Associate Professor, Department of Nuclear Engineering and Engineering Physics. Associate Fellow AIAA.

CB Control Coordinate System

An actuator configuration is assumed to have been chosen using an established placement technique.[9,10] The n physical DOF of the FEM are partitioned into two complementary sets: a with n_a DOF and o with n_o DOF, where the a set includes all actuator DOF. This results in an equation of motion for the free-free undamped structure of the form

$$\begin{bmatrix} M_{aa} & M_{ao} \\ M_{oa} & M_{oo} \end{bmatrix} \begin{Bmatrix} \ddot{\boldsymbol{x}}_a \\ \ddot{\boldsymbol{x}}_o \end{Bmatrix} + \begin{bmatrix} K_{aa} & K_{ao} \\ K_{oa} & K_{oo} \end{bmatrix} \begin{Bmatrix} \boldsymbol{x}_a \\ \boldsymbol{x}_o \end{Bmatrix} = \begin{Bmatrix} \boldsymbol{F}_a \\ 0 \end{Bmatrix} \tag{1}$$

where it has been assumed that loads are applied only at actuator locations. Considering the lower partition of the static portion of Eq. (1) and solving for the displacements of the o set in terms of the displacements of the actuator set, we obtain the relationship

$$\boldsymbol{x}_o = -K_{oo}^{-1} K_{oa} \boldsymbol{x}_a = \Psi \boldsymbol{x}_a \tag{2}$$

Constraining the actuator displacements to zero, a set of fixed actuator modes Φ can be obtained by solving the corresponding eigenproblem. The results of Eq. (2) and the fixed actuator modes can be combined into a set of displacement vectors, which can be used to generate a transformation from the original FEM configuration space of Eq. (1) to the CB coordinate space:

$$x = \begin{bmatrix} I_a & 0 \\ \Psi & \Phi \end{bmatrix} \begin{Bmatrix} \boldsymbol{x}_a \\ \boldsymbol{q} \end{Bmatrix} = T \boldsymbol{x}_{\mathrm{CB}} \tag{3}$$

The first partition of columns in Eq. (3) is static shapes called control constraint modes. Each of the columns represents the static deformation of the structure when one of the actuator locations is given a unit displacement while all other actuator locations are fixed. The second column partition contains the fixed actuator modes that describe the system dynamics relative to the actuators. The coordinate space of the CB representation contains the physical displacements of the actuators $\boldsymbol{x}_a$ and the modal displacements of the fixed actuator modes $\boldsymbol{q}$. The mass and stiffness matrices of the FEM representation are transformed using Eq. (3), resulting in the equation of motion

$$\begin{bmatrix} M_{aa} + \Psi^T M_{oa} + M_{ao}\Psi + \Psi^T M_{oo}\Psi & M_{ao}\Phi + \Psi^T M_{oo}\Phi \\ \Phi^T M_{oa} + \Phi^T M_{oo}\Psi & I_o \end{bmatrix} \times \begin{Bmatrix} \ddot{\boldsymbol{x}}_a \\ \ddot{\boldsymbol{q}} \end{Bmatrix} + \begin{bmatrix} K_{aa} + K_{ao}\Psi & 0 \\ 0 & \Lambda \end{bmatrix} \begin{Bmatrix} \boldsymbol{x}_a \\ \boldsymbol{q} \end{Bmatrix} = \begin{bmatrix} I_a \\ 0 \end{bmatrix} \boldsymbol{u} \tag{4}$$

or

$$\begin{bmatrix} \mathcal{M}_{aa} & \mathcal{M}_{ao} \\ \mathcal{M}_{oa} & I_o \end{bmatrix} \begin{Bmatrix} \ddot{\boldsymbol{x}}_a \\ \ddot{\boldsymbol{q}} \end{Bmatrix} + \begin{bmatrix} \mathcal{K}_{aa} & 0 \\ 0 & \Lambda \end{bmatrix} \begin{Bmatrix} \boldsymbol{x}_a \\ \boldsymbol{q} \end{Bmatrix} = \begin{bmatrix} I_a \\ 0 \end{bmatrix} \boldsymbol{u} \tag{5}$$

It has been assumed that the fixed actuator flexible mode shapes are mass normalized, i.e., $\Phi^T M_{oo} \Phi = I_o$ and $\Phi^T K_{oo} \Phi = \Lambda$, where $\Lambda = \text{diag}\{\lambda_1, \ldots, \lambda_Q\}$ is a diagonal matrix of the n_o fixed actuator mode eigenvalues. There are Q distinct eigenvalues, each with multiplicity n_q, so that $n_o = n_1 + n_2 + \cdots + n_Q$. Note that, if all of the fixed actuator modes are used in Eq. (3), Eqs. (1) and (5) are equivalent.

The full-order model (FOM) given by the CB representation may be reduced for control design and simulation using the EIM measure.[6] For simplicity, consider the case of collocated sensing. It has been shown that the following is a necessary and sufficient condition for controllability/observability.[11]

The CB equation of motion is controllable and observable if and only if

$$\rho(P_q) = n_q, \qquad q = 1, \ldots, Q \tag{6}$$

where n_q is the multiplicity of eigenvalue λ_q corresponding to Jordan block D_q ($q = 1, \ldots, Q$) of $D = \text{diag}\{0_{a \times a}, \Lambda\}$ and P_q is the corresponding row partition of the modal participation factor matrix $P = -[\Phi^T M_{oo} \Psi + \Phi^T M_{oa}]$.

The following EIM measure of controllability and observability has been proposed.[11]

Whenever Eq. (6) is satisfied, the controllability/observability measure of the ith fixed actuator mode is given by σ_i, the ith element of the $n_o \times 1$ EIM vector given by

$$\boldsymbol{\sigma} = \frac{1}{2} [\Sigma_{NT} \quad \Sigma_{NR}] \begin{Bmatrix} \mathbf{1} \\ \mathbf{1} \end{Bmatrix}$$

where

$$\Sigma = P^{\wedge^2} = \left[\Phi^T M_{oo} \Psi + \Phi^T M_{oa} \right]^{\wedge^2}$$

$$\Sigma_N = [\Sigma_T \quad \Sigma_R] \begin{bmatrix} \mathbf{1}_T & \mathbf{0}_T \\ \mathbf{0}_R & \mathbf{1}_R \end{bmatrix} \begin{bmatrix} \dfrac{1}{\text{tr}(\mathcal{M}_T)} & 0 \\ 0 & \dfrac{1}{\text{tr}(\mathcal{M}_R)} \end{bmatrix}$$

$$\mathcal{M} = \Psi^T M_{oa} + M_{ao} \Psi + \Psi^T M_{oo} \Psi + M_{ao} M_{oo}^{-1} M_{oa}$$

and where $[\ ]^{\wedge^2}$ indicates the term-by-term square, the subscript N refers to normalized, and T and R refer to translational and rotational DOF partitions, respectively.

The fixed actuator modes may be ranked using this measure, and the subset that contributes the desired amount to the completeness index is retained in the reduced model. The desired value is typically a percentage of the total such as 90%, i.e., $\Sigma \sigma_i = 0.9$. The EIM measure has been shown to be related to a popular control theoretic model reduction method based on the approximate balanced singular value (ABSV) for the case of acceleration input and actuator force output.[12] The ABSV represents the peak contribution of each mode to the maximum singular value of the transfer function. Selecting modes based on their ABSV, therefore, minimizes the peak magnitude (H_∞ norm) error of the transfer function. The EIM measure provides the same ranking of modes but offers the advantage that it is an absolute, as opposed to relative, measure of dynamic importance. In addition, it may be computed from simpler second-order-form matrix partitions and may easily be applied to vehicles that by definition possess rigid body modes. Additional information may be found in Ref. 12.

ESA Controller Design

Once the FOM has been reduced to a controllable/observable ROM, a control system is designed. To further exploit the second-order form of the equations of motion, the proposed control design is based on ESA for second-order systems.[7,8] Output feedback is particularly attractive for large systems because no estimation of state is required. We extend the presentation of Ref. 8 to include position and velocity sensing, leading to the control law $\boldsymbol{u} = -G\boldsymbol{y} = -G_p C_p \boldsymbol{x} - G_v C_v \dot{\boldsymbol{x}}$. This control law is then substituted into the CB ROM equation of motion

$$M\ddot{\boldsymbol{x}} + D\dot{\boldsymbol{x}} + K\boldsymbol{x} = \bar{B}\boldsymbol{u} \tag{7}$$

and the following eigenproblem is formed:

$$\Gamma_i \boldsymbol{\phi}_i \equiv 0 \tag{8}$$

where

$$\Gamma_i = \left[\lambda_i^2 M + \lambda_i D + K \ \vdots \ \bar{B} \right] \tag{9}$$

$$\boldsymbol{\phi}_i = \begin{bmatrix} \bar{\phi}_i \\ \hat{\phi}_i \end{bmatrix} \triangleq \begin{bmatrix} \boldsymbol{\nu}_i \\ (G_p C_p + \lambda_i G_v C_v) \boldsymbol{\nu}_i \end{bmatrix} \tag{10}$$

for $i = 1, \ldots, p$, where p is the number of assigned eigenvalues λ_i, and $\boldsymbol{\nu}_i$ are eigenvectors.

The design process is carried out by assigning the desired closed-loop eigenvalue λ_i^d and computing the corresponding null space V_{0_i} of the matrix Γ_i using singular-value decomposition. Noting that any linear combination of the vectors contained in this null space also satisfies Eq. (8), we may express

$$\begin{bmatrix} \bar{\phi}_i \\ \hat{\phi}_i \end{bmatrix} = V_{0_i} \boldsymbol{l}_i \tag{11}$$

where $\boldsymbol{l}_i$ is an $n_a \times 1$ vector of linear combination coefficients chosen by the designer and n_a is the number of actuators. Observe that the upper partition of Eq. (11), $\bar{\phi}_i$, is the ith closed-loop eigenvector. This gives the designer freedom to assign eigenvector elements by choice of the linear combination coefficients. This process is carried out for all p eigenvalues. By inspection of Eq. (10), the design equation is given by

$$G_v C_v \bar{\Phi} \Lambda + G_p C_p \bar{\Phi} = \hat{\Phi} \tag{12}$$

where

$$\bar{\Phi} = \left[\bar{\phi}_1 \quad \bar{\phi}_2 \quad \cdots \quad \bar{\phi}_p \right], \qquad \hat{\Phi} = \left[\hat{\phi}_1 \quad \hat{\phi}_2 \quad \cdots \quad \hat{\phi}_p \right]$$

and

$$\Lambda = \text{diag}(\lambda_i), \qquad i = 1, \ldots, p$$

Separating this into real and imaginary components, the design equation becomes

$$[G_v \quad G_p] \begin{bmatrix} C_v & 0 \\ 0 & C_p \end{bmatrix} \begin{bmatrix} \bar{\Phi}_r \Lambda_r - \bar{\Phi}_i \Lambda_i & \bar{\Phi}_r \Lambda_i + \bar{\Phi}_i \Lambda_r \\ \bar{\Phi}_r & \bar{\Phi}_i \end{bmatrix} = [\hat{\Phi}_i \quad \hat{\Phi}_r]$$

where the subscripts r and i denote real and imaginary, respectively. This may be compactly written as

$$G \bar{C} \bar{\Upsilon} = \hat{\Upsilon} \tag{13}$$

from which the gain matrix is obtained by pseudoinverse as $G = \hat{\Upsilon}(\bar{C}\bar{\Upsilon})^\dagger$.

Closed-Loop Behavior

In this section we investigate the proposed fixed actuator CB representation in ROM-based control design applications. The performance of the fixed actuator CB representation will be compared with the common normal mode (or modal) representation. The use of fixed mode over free mode models in closed-loop applications is motivated by the fact that a reduced free mode model will not accurately represent boundary conditions where loads are applied to the structure.[13] In the proposed CB modeling approach, fixed modes are calculated with respect to fixed actuator locations. Constraint modes, containing a statically complete reduced representation, are

then appended to these fixed modes, providing complete flexibility from the actuator locations. In contrast, the normal mode representation computes the modes with actuator locations free. When a reduced set of normal modes is retained in modeling, a significant amount of local flexibility may be neglected, resulting in an inability to accurately represent boundary conditions at actuator locations where forces are applied. This is particularly true when actuator commands are large and the actuator boundary conditions become more rigid.

To better understand static completeness in the CB representation, consider the system receptance[4] of a physical FEM representation with collocated position sensing. This is given by the expression

$$H(\omega) = C_p(K + j\omega D + \omega^2 M)^{-1}\bar{B} \tag{14}$$

The static receptance is then defined by

$$\lim_{\omega \to 0} H(\omega) = C_p K^{-1}\bar{B} = \left(K_{aa} - K_{ao}K_{oo}^{-1}K_{oa}\right)^{-1} \tag{15}$$

This quantity is recognized as the inverse of the a set stiffness partition of the CB representation, which is always preserved if the control constraint modes are retained. Even when no fixed actuator modes are retained, the receptance of the reduced CB model is exact and, thus, the static actuator loads are preserved. This implies the input to output behavior of the reduced CB model will be exact as $\omega \to 0$. For the normal mode model with collocated position sensors, the static receptance may be expressed as

$$\lim_{\omega \to 0} H(\omega) = \left[K_f - K_f\phi_{ar}\left(\phi_{ar}^T K_f \phi_{ar}\right)^{-1}\phi_{ar}^T K_f\right]^{-1} \tag{16}$$

where $K_f = \phi_{af}\Lambda_f^{-1}\phi_{af}^T$, $\phi_a = [\phi_{ar}\ \ \phi_{af}]$ is the a set partition of the normal modes separated into rigid body modes (zero frequency) and flexible modes, respectively; and Λ_f^{-1} is the flexible mode partition of the frequency matrix. We see that in this case the receptance depends explicitly on the a set partition of the normal modes and will only be exact when all of the normal modes are retained. Reduced-order normal mode models, thus, will be stiff from the actuator locations. It would be reasonable to expect the control design to overpredict the required control gain magnitudes. This will result in inaccurate actuation forces used by the controller to modify the open-loop response. Note that the open-loop eigenvalues of the modal ROM will be exact, whereas the CB model open-loop eigenvalues will not. The CB ROM errors are predominantly found in higher-frequency modes, which allows good performance for low-frequency bandwidth applications. Even though the open-loop eigenvalues of the CB ROM are less accurate than the normal mode ROM, we will see that the closed-loop accuracy is substantially improved due to the more accurate actuation commands.

A general block diagram for a feedback system containing a reference input $r(s)$ and a disturbance input $w(s)$ is shown in Fig. 1 in terms of Laplace variables. The controller is denoted by $K(s)$ and the plant by $P(s)$. For simplicity, consider a single-input/single-output system and the proportional-plus-derivative controller given by $K(s) = k_p + sk_v$. The transfer functions, in pole-zero form, from the reference signal to the output, the disturbance to the output, and the disturbance to the control are given by

$$\frac{y(s)}{r(s)} = \frac{(k_p + sk_d)\prod_{i=1}^{n_z}(s - z_i)}{\prod_{i=1}^{n_p}\left(s - p_i^{\mathrm{cl}}\right)} \tag{17}$$

$$\frac{y(s)}{w(s)} = \frac{\prod_{i=1}^{n_p}(s - p_i)}{\prod_{i=1}^{n_p}\left(s - p_i^{\mathrm{cl}}\right)} \tag{18}$$

$$\frac{u(s)}{w(s)} = \frac{(k_p + sk_d)\prod_{i=1}^{n_p}(s - p_i)}{\prod_{i=1}^{n_p}\left(s - p_i^{\mathrm{cl}}\right)} \tag{19}$$

where z_i and p_i are the open-loop zeros and poles of the plant, respectively, and p_i^{cl} are the closed-loop poles. Based on our argument that the fixed actuator modes lead to improved actuator boundary

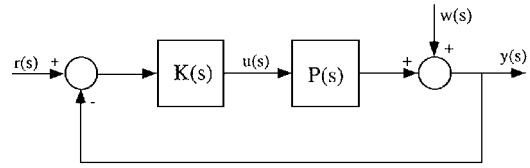

Fig. 1 General feedback block diagram.

conditions and actuation forces, it is hypothesized that the denominators (closed-loop poles) of the preceding transfer functions are more accurate for the fixed-mode representation. The zeros of the transfer function in Eq. (17) are the open-loop zeros of the plant. By definition, the exact open-loop zeros of the plant are frequencies at which the plant can be excited at the input with no resulting output. These are the fixed actuator mode frequencies. Thus, the fixed-mode representation will lead to a more accurate numerator for this transfer function than the modal model. Conversely, for the transfer function of Eqs. (18) and (19), the zeros are the open-loop poles of the plant and, thus, the normal mode model will be more accurate. However, the open-loop poles are typically very lightly damped, and so we would expect the improved behavior in the normal mode representation to occur only at isolated frequencies. In general, the preceding transfer functions will be more accurate for the CB representation at all but isolated frequencies near the open-loop poles of the plant, as discussed by Blelloch and Carney.[13]

In the control design process just discussed, the FOM is partitioned into retained r and truncated t DOF, i.e.,

$$\boldsymbol{x} = \begin{Bmatrix} \boldsymbol{x}_r \\ \cdots \\ \boldsymbol{x}_t \end{Bmatrix}$$

where $\boldsymbol{x}_t$ are a subset of the fixed actuator modal coordinates $\boldsymbol{q}$. The associated matrices in Eq. (7) expanded into the retained and truncated partitions are given by

$$M \triangleq \begin{bmatrix} M_{rr} & M_{rt} \\ M_{tr} & M_{tt} \end{bmatrix}, \qquad D \triangleq \begin{bmatrix} D_{rr} & 0 \\ 0 & D_{tt} \end{bmatrix}$$

$$K \triangleq \begin{bmatrix} K_{rr} & 0 \\ 0 & K_{tt} \end{bmatrix}, \qquad \bar{B} \triangleq \begin{bmatrix} \bar{B}_r \\ 0 \end{bmatrix}$$

$$C_p \triangleq [C_{pr} \quad C_{pt}], \qquad C_v \triangleq [C_{vr} \quad C_{vt}]$$

and the closed-loop FOM is given by the expression

$$\begin{bmatrix} M_{rr} & M_{rt} \\ M_{tr} & M_{tt} \end{bmatrix}\begin{Bmatrix} \ddot{\boldsymbol{x}}_r \\ \ddot{\boldsymbol{x}}_t \end{Bmatrix} + \begin{bmatrix} D_{rr} + \bar{B}_r G_v C_{vr} & \bar{B}_r G_v C_{vt} \\ 0 & D_{tt} \end{bmatrix}\begin{Bmatrix} \dot{\boldsymbol{x}}_r \\ \dot{\boldsymbol{x}}_t \end{Bmatrix}$$

$$+ \begin{bmatrix} K_{rr} + \bar{B}_p G_r C_{pr} & \bar{B}_r G_p C_{pt} \\ 0 & K_{tt} \end{bmatrix}\begin{Bmatrix} \boldsymbol{x}_r \\ \boldsymbol{x}_t \end{Bmatrix} = \begin{Bmatrix} \boldsymbol{0} \\ \boldsymbol{0} \end{Bmatrix} \tag{20}$$

Control design is carried out on the system defined by the upper partition neglecting coupling terms, i.e.,

$$M_{rr}\ddot{\boldsymbol{x}}_r + D_{rr}\dot{\boldsymbol{x}}_r + K_{rr}\boldsymbol{x}_r = -\bar{B}_r G_v C_{vr}\dot{\boldsymbol{x}}_r - \bar{B}_r G_p C_{pr}\boldsymbol{x}_r \tag{21}$$

which defines the reduced-order design model. When the resulting control gains are applied to the full-order system, eigenstructure error results from neglecting the coupling terms in the design process. These coupling terms are commonly referred to in the literature as spillover. Examination of Eq. (20) reveals the presence of two forms of spillover. Dynamic spillover results from the presence of the mass coupling term $M_{rt} = M_{tr}^T$ appearing in both the retained and truncated DOF partitions. A combination of control/observation spillover is produced by the terms $\bar{B}_r G_v C_{vt}$ and $\bar{B}_r G_p C_{pt}$ present in the retained DOF partition.

In the absence of these coupling terms, the controller designed using the ROM, when applied to the full model, will be exact, providing the precise desired eigenstructure. Recall that the modal participation factor matrix is defined as

$$P \triangleq \Phi^T M_{oo}\Psi + \Phi^T M_{oa} \tag{22}$$

Separating the fixed actuator modal coordinates into retained and truncated DOF, the modal participation factor matrix may be partitioned as

$$P \triangleq \begin{bmatrix} P_r \\ P_t \end{bmatrix} = \begin{bmatrix} \Phi_r^T M_{oo} \Psi + \Phi_r^T M_{oa} \\ \Phi_t^T M_{oo} \Psi + \Phi_t^T M_{oa} \end{bmatrix} \tag{23}$$

Using this notation, the reduced interior mass matrix[6] may be expressed as

$$\mathcal{M} = P^T P = P_r^T P_r + P_t^T P_t \tag{24}$$

By the preceding definitions, we recognize that $M_{\text{tr}} \equiv P_t$. The trace norm of the mass coupling matrix is defined by

$$\|M_{\text{tr}}\| = \sum_{i=1}^{n_t} \sigma_i^{\frac{1}{2}} \tag{25}$$

where σ_i are the singular values of $M_{\text{tr}}^T M_{\text{tr}} = P_t^T P_t$. Thus, by retaining the fixed actuator modes with the largest contribution to the trace norm of the reduced interior mass matrix, we are minimizing the trace norm of the mass coupling matrix. By retaining fixed actuator modes with large EIM measures, we are ensuring that the dynamic spillover, as well as potential closed-loop instability, is minimized. If all of the EIM is retained, the dynamic spillover will identically vanish. If collocated sensors alone are used, the control/observation spillover terms will also vanish, i.e., C_{vt} and $C_{pt} \equiv 0$. In this case, the closed-loop FOM is block diagonal and the eigenproblem for the reduced controller design is implemented exactly.

For the normal mode representation, no absolute measure exists for reducing the model to ensure that spillover and potential destabilization are minimized. Balas[14] has discussed spillover phenomena for normal mode representations. The normal mode representation possesses no dynamic spillover, but observation spillover is present even if sensors are strictly collocated. The eigenproblem will only be uncoupled if no modes are truncated or additional signal processing is introduced.[15]

Cantilever Beam Example

An ESA control design is now carried out for a 10-node, 10-element cantilever beam with rotational and translational DOF. A schematic of the FEM is shown in Fig. 2, along with the actuator and sensor locations. A normal mode model and a CB representation with the actuators fixed are formed. It is desired to control the first two bending modes (19.95 and 125.04 Hz) of the cantilever. This defines the necessary ROM bandwidth. The CB model is reduced using the EIM measure, which retains fixed actuator modes 1 and 3 as well as the two constraint modes. The normal mode representation is reduced by retaining the lowest four modes. Having reduced the CB model using EIM, controllability and observability are guaranteed. These conditions are tested for the normal mode model and found to be satisfied.

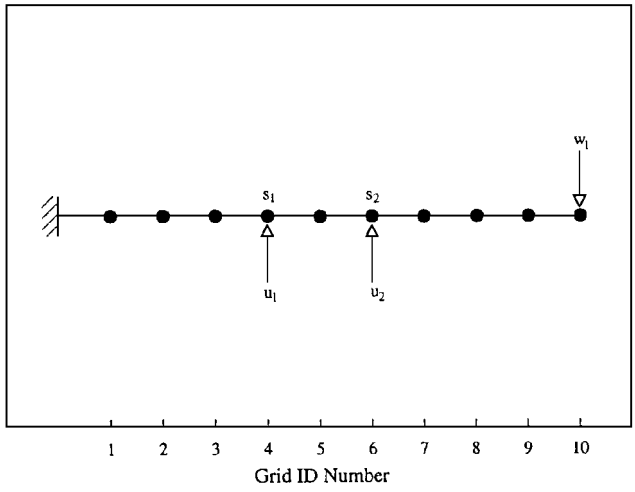

Fig. 2 Cantilever beam example.

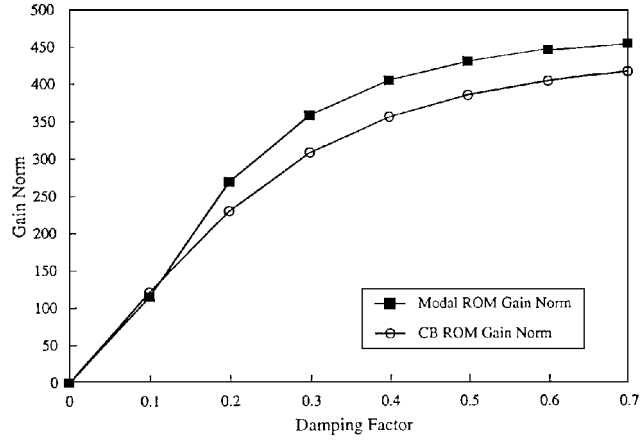

Fig. 3 Gain norm vs damping factor.

A controller will be designed for each ROM and then applied to the FOM to compute resulting implementation errors. The control objectives will be to increase damping factors in the control target modes and constrain the tip displacement and rotations of the corresponding eigenvectors to $\frac{1}{10}$ of the open-loop values. The damping factors are increased while preserving the modal frequency. This is accomplished by rotating the undamped poles off the imaginary axis in circular paths as specified in the design process by the desired closed-loop eigenvalue.

It is expected that as gain magnitude increases, the CB ROM performance will increase relative to the normal mode model. If the Frobenious norm of the gain is plotted vs the damping factor we see the gain norm increases with increasing damping factor providing this comparison. This is shown in Fig. 3. The normal mode ROM gain is seen to be larger than CB ROM gain norm in all but the $\zeta = 0.1$ design. This is consistent with the observation that the normal mode ROM is stiffer than the statically complete CB ROM. For the $\zeta = 0.1$ design point, the desired eigenvalues and the desired eigenvectors are more consistent in the normal mode ROM than in the CB ROM in that they produce a better conditioned set of target eigenvectors for the inverse in the design equation; thus the lower gain norm. We now make our comparisons by varying the damping factors and keep in mind that higher damping factors translate into larger control gains and thus larger constraint forces at the actuator locations.

Closed-Loop Eigenvalue Accuracy

The s-plane eigenvalue errors for both ROM designs are computed for the two target control modes by defining the relative s-plane error as

$$\text{error}(\%) = \frac{|s - s'|}{|s|} \times 100\% \tag{26}$$

which represents a normalized distance from the exact location s to the approximate location s'. The exact location corresponds to the value obtained in full-order implementation, and the approximate location corresponds to the ROM predicted location. A plot of the errors vs damping factor is shown in Fig. 4. The CB ROM errors are smaller for all designs, including the $\zeta = 0.1$ design point, and in fact do not exceed 2% error. The normal mode ROM design errors are seen to become excessively large for damping factors above 0.3.

Closed-Loop Eigenvector Accuracy

To investigate how close the obtained eigenvector is to the desired eigenvector, the s plane desired and actual displacement element locations for the control modes are computed. A single measure of a mode's gross error may be computed by taking the square root of the sum of square errors of these vectors. Figure 5 shows the two control modes' displacement rss error vs damping factor. Note that the $\zeta = 0.1$ design point is more accurate for the normal mode ROM, but for all other design points, the CB ROM eigenvectors are much more accurately assigned. In this example, tip displacement and rotations of the two target eigenvectors were assigned to be $\frac{1}{10}$ of the open-loop values; next consider the tip displacement errors

individually. The errors are shown in Figs. 6 and 7 and represent the percentage difference in s-plane location from that desired in the design. The CB ROM controller is seen to produce much more accurate closed-loop eigenvector tip elements than the normal mode ROM controller. Note that in Fig. 6 the CB amplitude and phase errors overlay each other.

Next consider left eigenvector assignment accuracy. A controller is to be designed to reject the tip disturbance w_1, which is assumed to act at low frequencies and primarily disturb modes 1 and 2. The control design objectives are to provide 10% damping in the first two modes, without changing modal frequency, and to assign the left eigenvectors such that they are nearly orthogonal to the disturbance influence matrix. This last objective will reject the disturbance. The disturbance influence matrix will contain a single 1 in the row corresponding to the tip displacement, so that it is within design

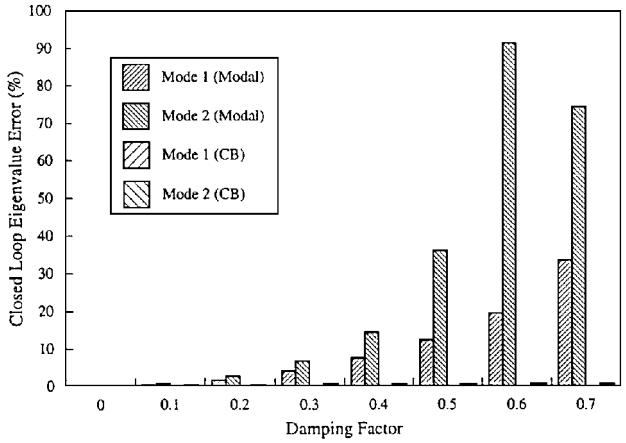

Fig. 4 Closed-loop eigenvalue s-plane error vs damping factor.

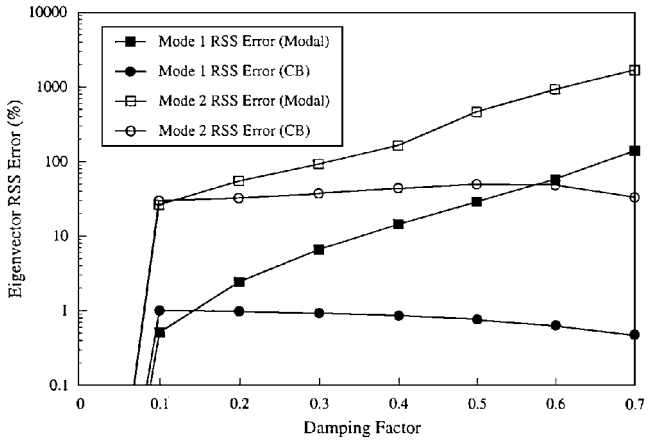

Fig. 5 Displacement eigenvector s-plane rss error.

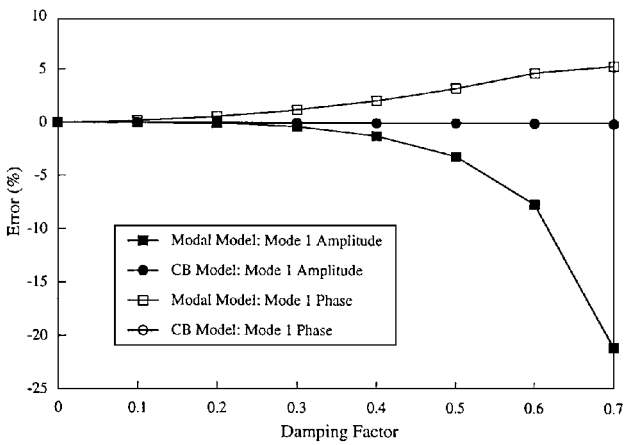

Fig. 6 Mode 1 tip displacement error.

Table 1 Left eigenvector assignment disturbance rejection comparison

Mode	$l_i^T \bar{\Gamma}$	λ^d	λ^{act}
		Open loop	
1	39.26	N/A	$\pm j19.95$
2	98.31	N/A	$\pm j125.04$
		Normal mode	
1	32.61	$-2 \pm j19.85$	$-0.41 \pm j45.26$
2	62.10	-12 ± 124.41	$-50.64 \pm j131.39$
		CB	
1	0.03	$-2 \pm j19.85$	$-2 \pm j19.85$
2	7.719	-12 ± 124.41	$-12.43 \pm j124.30$

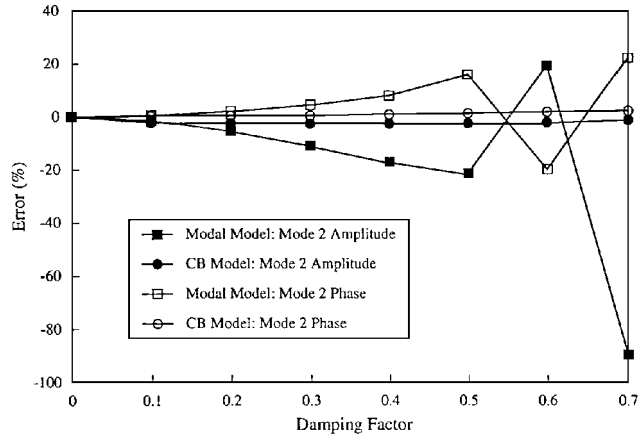

Fig. 7 Mode 2 tip displacement error.

constraints to assign a zero element to each of the control target modes in the corresponding row. In this example, the ROMs contain six modes, by necessity, to provide stable designs. The eigenvector tip displacement is assigned a magnitude of $1e{-}5$ times the open-loop magnitude, and the tip rotation is assigned its open-loop value. Comparisons are shown in Table 1. The table shows the desired (target) eigenvalues λ^d and those actually obtained in implementation λ^{act} on the FOM. Again we find much more accurate attainment of the desired closed-loop eigenvalues for the CB ROM-based design. The table also shows the projection of the obtained left eigenvector onto the disturbance influence matrix $l_i^T \bar{\Gamma}$. If this is zero, the disturbance has no effect on the transient response of the system. Small values of this projection indicate higher accuracy of the left eigenvector assignment. We again observe that the CB ROM is substantially more accurate in specification of eigenvector elements.

Transfer Function Accuracy

Next, consider the accuracy of the closed-loop transfer functions obtained using the four-mode ROMs in the ESA control design process. Transfer function s-plane errors from actuator 1 to sensor 1 and actuator 2 to sensor 2 are plotted in Fig. 8 for a damping factor of 0.4. The errors are computed using the relation

$$\text{Error}(\%) = \frac{|H(s) - H(s)'|}{|H(s)|} \times 100\% \tag{27}$$

where $H(s)$ is the FOM implementation and prime denotes a ROM implementation. Note that a value in Fig. 8 of -20 dB represents a 1% error in the s-plane location. We see that the CB design leads to improved accuracy over the entire control bandwidth of approximately 125 rad/s, the only exceptions in narrow-frequency bands as expected.

Stability Behavior

Eigenstructure assignment using output feedback does not, in general, guarantee closed-loop stability. Therefore, it is important that the ROM accurately predict closed-loop instability. It has been shown that reduced normal mode models tend to overpredict the required gain norm. When this larger gain is then applied to the FOM, there is the potential for destabilization due to spillover

into unmodeled dynamics that was not predicted in the ROM. Indeed if a controller is designed for the four-mode ROMs assigning $\lambda_1^d = -30 \pm j30$ and $\lambda_2^d = -25 \pm j125$, along with the eigenvector design constraints that the corresponding eigenvector tip displacement and rotation be $\frac{1}{10}$ of their open-loop values, we find that the closed-loop normal mode ROM ($\|G\|_F = 310.6$) is stable but that implementation of the controller on the FOM destabilizes an unmodeled mode. The corresponding CB design ($\|G\|_F = 284.5$) is stable in both cases.

Design experience using the CB representation indicates that, in general, stable ROM behavior leads to stable FOM implementation and vice versa. This has been found to be much less the rule for the normal mode representation due to its tendency to overpredict the necessary control gain magnitudes.

Control-Structures Interaction Example

For the proposed control design process to be truly useful, it must be easily and effectively implementable on realistic systems. In this section an example is given for the test-correlated FEM of the controls-structures interaction (CSI) evolutionary model testbed at the NASA Langley Research Center (LaRC) Space Structures Research Laboratory.[3] The FEM of the CSI structure is shown in Fig. 9 and consists of 482 grid points with 6 DOF per grid for a total of 2892 DOF. The structure is supported by two cable systems attached to the forward and aft suspension trusses. The FEM was test correlated by NASA LaRC to accurately predict 27 mode shapes and frequencies below 35 Hz. For efficiency, the model was statically reduced to 41 DOF that accurately predict the structure's low-frequency dynamics. Thrust force devices are used as actuators at eight locations with collocated position and rate sensors, and eight additional position/rate sensors are placed in noncollocated positions. The additional noncollocated sensors are added to provide small, minimum norm, solutions of the eigenstructure assignment design equations. The sensor S and actuator A locations and directions are identified by arrows in Fig. 9.

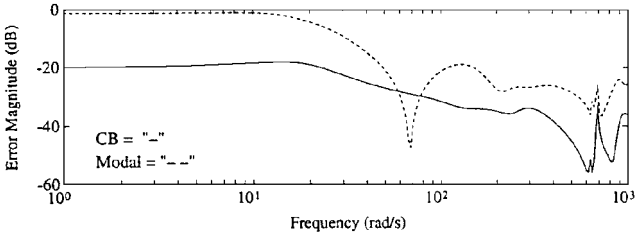

Actuator 1 to sensor 1

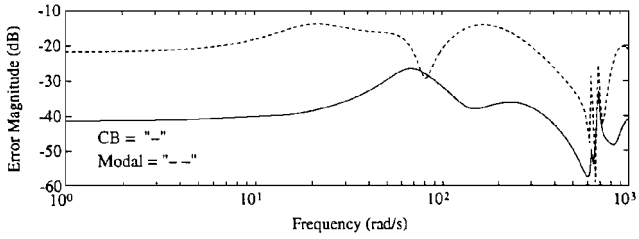

Actuator 2 to sensor 2

Fig. 8 Transfer function errors for $\zeta = 0.4$.

The control objective will be to augment stiffness and damping in the first six suspension modes and the first Y-bending and first X-torsional mode of the structure. A description and the undamped natural frequencies of these modes are listed in Table 2. An additional objective will be to reduce a line-of-sight (LOS) response based on relative tower-to-tower low-frequency motion by eigenvector shaping. The path from DOF 310 to DOF 267 defines the LOS shown by the dashed line in Fig. 9. The reduced FEM is transformed to a CB representation with the actuators fixed and into a normal mode model. Based on EIM controllability/observability measures, the CB representation is then reduced to the eight control constraint modes and the first eight fixed actuator modes, which contribute 88.8% of the trace of the reduced interior mass matrix.[3] The normal mode model is reduced to the 16 lowest-frequency modes. The ROMs are assumed to have intrinsic, stiffness proportional damping with a proportionality constant of 1/1000. The open-loop and target closed-loop pole locations and corresponding damping factors for the eight target modes of the FOM are given in Table 3. The suspension mode eigenvectors will be targeted to be the least squares projection of the open-loop eigenvectors on the achievable eigenvector subspace of the corresponding desired closed-loop eigenvalues. The two flexible target modes will be shaped to have zero displacement at reflector tower DOF 267 and laser tower DOF 310 to minimize the LOS error.

Table 2 CSI control target mode descriptions

Target mode description	Frequency, Hz	Frequency, rad/s
Cable pendulum	0.112	0.704
Cable pendulum	0.112	0.704
Cable twist pendulum	0.129	0.811
Cable axial	0.825	5.184
Cable junction bending	0.959	6.025
Cable axial	0.963	6.051
First X torsion	1.809	11.366
First Y bending	3.129	19.660

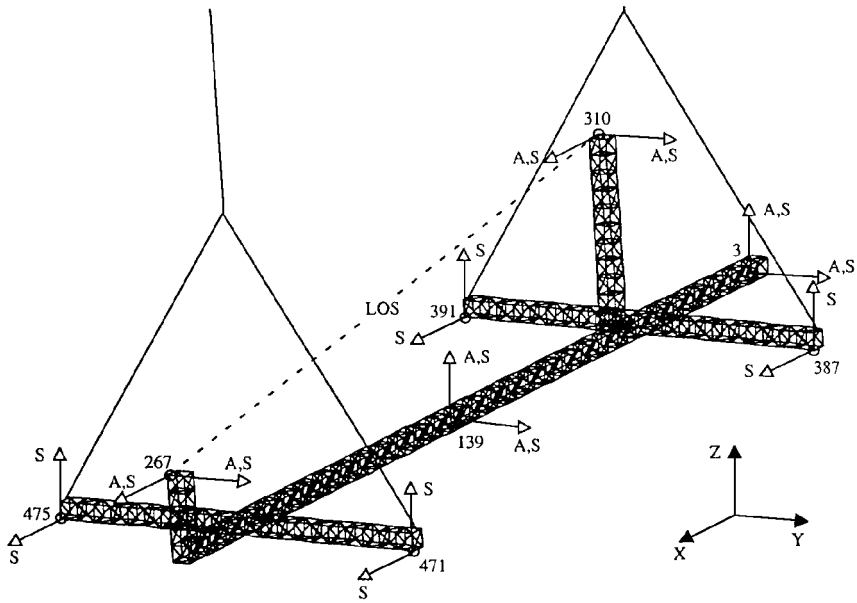

Fig. 9 CSI finite element model.

Table 3 Target mode *s*-plane open-loop and desired pole locations

OL pole location	ζ^{ol}	Target pole location	ζ^{d}
$-2.486e{-}4 \pm j0.705$	0.0004	$-1 \pm j1$	0.7071
$-2.492e{-}4 \pm j0.706$	0.0004	$-2 \pm j2$	0.7071
$-3.305e{-}4 \pm j0.813$	0.0004	$-3 \pm j3$	0.7071
$-1.342e{-}2 \pm j5.181$	0.0026	$-2 \pm j4$	0.4472
$-1.815e{-}2 \pm j6.025$	0.0030	$-3 \pm j5$	0.5145
$-1.829e{-}2 \pm j6.049$	0.0030	$-5 \pm j6$	0.6402
$-6.457e{-}2 \pm j11.363$	0.0057	$-10 \pm j12$	0.6402
$-1.930e{-}1 \pm j19.658$	0.0098	$-12 \pm j20$	0.5145

Table 4 CB ROM controller actual pole locations and errors

Pole location	Error, %
$-0.9984 \pm j0.9991$	0.129
$-1.9999 \pm j2.0001$	0.005
$-2.9973 \pm j2.9980$	0.079
$-1.9997 \pm j4.0011$	0.025
$-2.9990 \pm j5.0039$	0.069
$-4.9972 \pm j6.0044$	0.067
$-9.9990 \pm j12.0680$	0.435
$-11.5240 \pm j20.6000$	3.284

Table 5 Normal mode ROM controller actual pole locations and errors

Pole location	Error, %
$-0.9977 \pm j1.0153$	1.094
$-2.0006 \pm j2.0043$	0.154
$-3.3972 \pm j3.1676$	10.161
$-1.9881 \pm j3.9969$	2.275
$-2.4699 \pm j4.8300$	9.547
$-4.9753 \pm j5.9618$	0.582
$-11.5630 \pm j10.0630$	15.826
$-11.0740 \pm j15.1190$	21.428

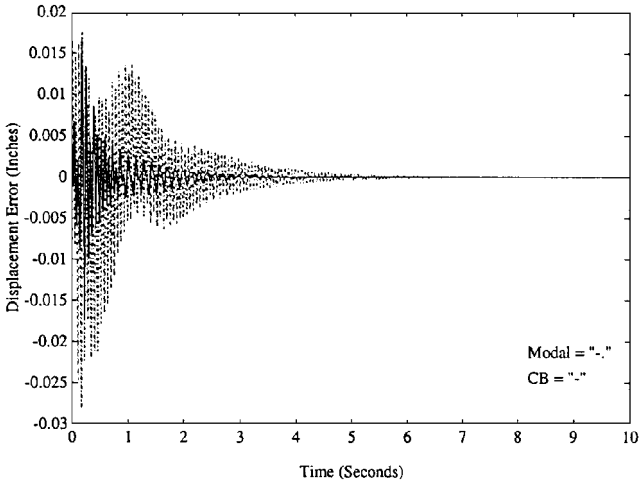

Fig. 10 LOS displacement response prediction error comparison: impulse at 139*Z*.

Control design is carried out using the eigenstructure assignment algorithm for output feedback on the CB ROM and normal mode ROM. Both ROM are found to be stable. The resulting gain matrices are then applied to the FOM, and the eigenstructure is compared to the desired. The ROM and FOM pole locations and *s*-plane error percentages are listed in Tables 4 and 5. The CB ROM gain matrix is found to have a Frobenious norm of 23.94, and the normal mode ROM has a Frobenious norm of 95.1. Again, the normal mode ROM is stiff, resulting in overestimation of the required control forces. The CB ROM controller places all of the control target mode eigenvalues accurately; the largest error is less than 4%. The normal mode ROM, however, has maximum pole placement errors exceeding 20%; three modes with errors greater than 10%. LOS

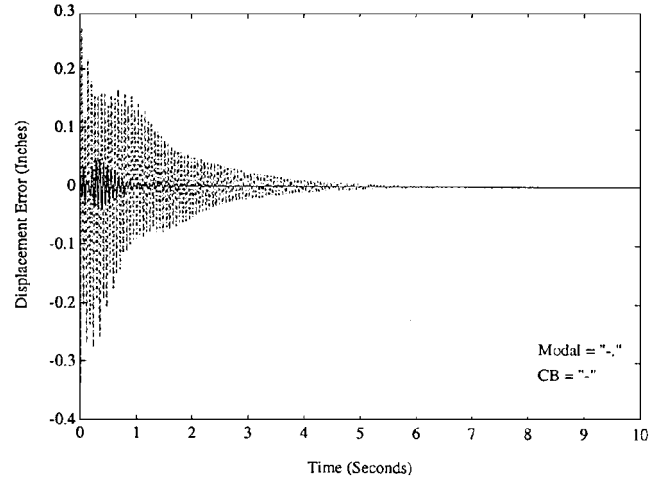

Fig. 11 LOS displacement response prediction error comparison: impulse at 267*Y*.

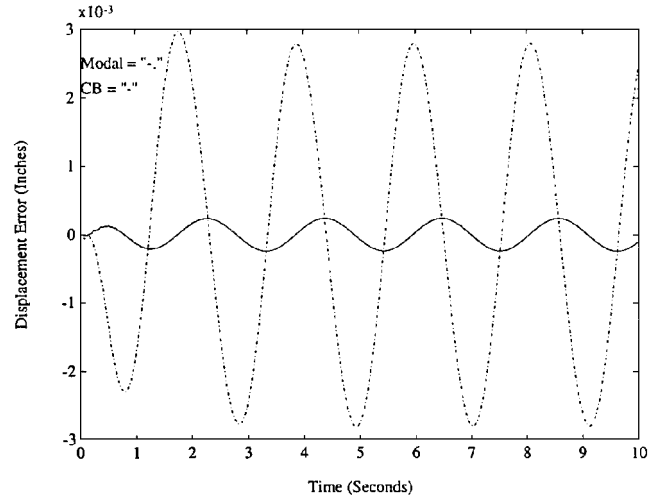

Fig. 12 LOS displacement response prediction error comparison: 3-rad/s dwell at 267*Y*.

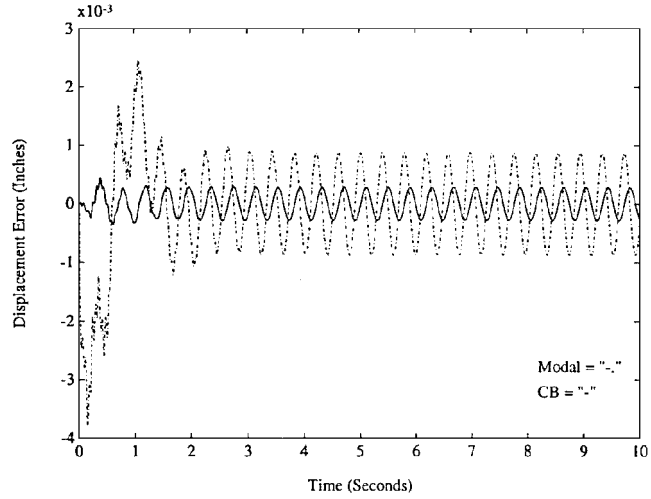

Fig. 13 LOS displacement response prediction error comparison: 16-rad/s dwell at 267*Y*.

response prediction errors for the ROM are shown in Figs. 10 and 11 for a unit impulse applied to DOF 139*Z* and DOF 267*Y*, respectively, demonstrating the CB ROM improved prediction accuracy. Next, DOF 267*Y* LOS transient response is calculated for unit amplitude steady-state sinusoidal disturbances at 3 and 16 rad/s. The LOS displacement error comparisons are shown in Figs. 12 and 13 and again show the benefits of the CB ROM design. The rectified open- and closed-loop responses of the CB ROM-based controller

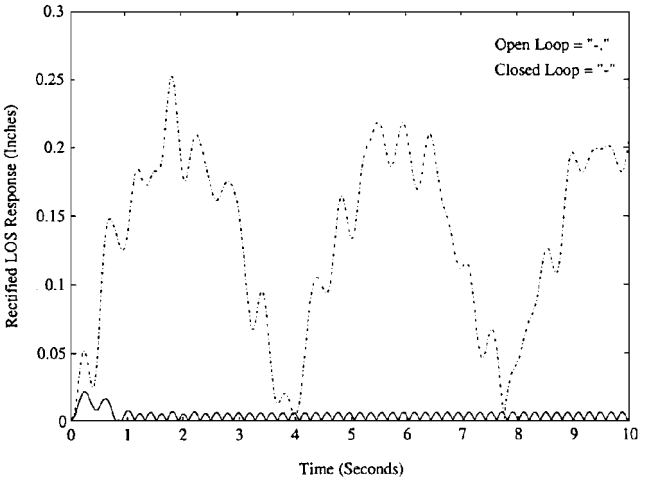

Fig. 14 Open- and closed-loop LOS displacement responses for CB ROM-based control design: 16-rad/s dwell at 267*Y*.

are shown in Fig. 14 for the 16-rad/s disturbance, demonstrating the effectiveness of eigenvector shaping in reducing LOS response.

Conclusion

The use of substructure representations in conjunction with modern control system design methodologies provides a simple and accurate approach to reduction of large-scale structural control problems. The proposed control coordinate system based on the CB substructure representation has been shown to produce more accurate closed-loop behavior when used in ROM-based eigenstructure assignment controller design applications than conventional normal mode modeling approaches. The CB ROM's ability to accurately predict required actuation commands improves the ROM stability prediction of the closed-loop system as well. Extensions of this modeling approach to include fixed interface DOF as well as fixed actuator/sensor DOF are currently being investigated. These extensions will allow the synthesis of both the structure and the controller using a single aggregation methodology that will retain useful measures of modal dynamic importance, controllability, and observability at the coupled and the substructure level of the design.

Acknowledgments

The first author gratefully acknowledges the support of NASA through the National Space Grant College and Fellowship Program and the Wisconsin Space Grant Consortium and would also like to thank the TRW Space and Electronics Group for their continued support.

References

[1] Su, T. J., and Craig, R. R., Jr., "Substructuring Decomposition and Controller Synthesis," *Proceedings of the AIAA/ASME/ASCE/AHS/ASC 31st Structures, Structural Dynamics, and Materials Conference* (Long Beach, CA), AIAA, Washington, DC, 1990, pp. 1932–1940 (AIAA Paper 90-1039).

[2] Babuška, V., and Craig, R. R., Jr., "Substructure-Based Control of Flexible Structures," *Proceedings of the AIAA/ASME/AHS/ASC 34th Structures, Structural Dynamics, and Materials Conference* (La Jolla, CA), AIAA, Washington, DC, 1993, pp. 3415–3421.

[3] Triller, M. J., "A Substructural Approach to the Control of Large Space Structures," Ph.D. Thesis, Dept. of Engineering Mechanics and Astronautics, Univ. of Wisconsin, Madison, WI, Aug. 1994.

[4] Alvin, K. F., Park, K. C., and Peterson, L. D., "A Consistent Model Reduction of Measured Modal Parameters for Reduced-Order Active Control," Center for Space Structures and Controls, Rept. CU-CSSC-93-15, Univ. of Colorado, Boulder, CO, June 1991.

[5] Craig, R. R., Jr., and Bampton, M. C. C., "Coupling of Substructures for Dynamic Analysis," *AIAA Journal*, Vol. 6, No. 7, 1968, pp. 1313–1319.

[6] Kammer, D. C., and Triller, M. J., "Ranking the Dynamic Importance of Fixed Interface Modes Using a Generalization of Effective Mass," *International Journal of Analytical and Experimental Modal Analysis*, Vol. 9, No. 2, 1994, pp. 77–98.

[7] Rew, D. W., Junkins, J. L., and Juang, J. N., "Robust Eigenstructure Assignment by a Projection Method: Applications Using a Multiple Optimization Criteria," *Journal of Guidance, Control, and Dynamics*, Vol. 12, No. 3, 1989, pp. 396–403.

[8] Juang, J. N., and Maghami, P. G., "Robust Eigensystem Assignment for Second-Order Dynamic Systems," *Mechanics and Control of Large Flexible Structures*, edited by J. L. Junkins, Vol. 129, Progress in Astronautics and Aeronautics, AIAA, Washington, DC, 1990, pp. 373–387.

[9] Juang, J. N., and Rodriguez, G., "Formulations and Applications of Large Structure Actuator and Sensor Placements," *Proceedings of the 2nd VPI&SU/AIAA Symposium on Dynamics and Control of Large Flexible Spacecraft*, Blacksburg, VA, 1979, pp. 247–262.

[10] Kim, Y., and Junkins, J. L., "Measures of Controllability for Actuator Placement," *Journal of Guidance, Control, and Dynamics*, Vol. 14, No. 5, 1991, pp. 895–902.

[11] Triller, M. J., and Kammer, D. C., "Controllability and Observability Measures for Craig–Bampton Substructure Representations," *Journal of Guidance, Control, and Dynamics*, Vol. 17, No. 6, 1991, pp. 1198–1204.

[12] Kammer, D. C., and Triller, M. J., "Selection of Component Modes for Craig–Bampton Representations," *Journal of Vibrations and Acoustics*, Vol. 118, April 1996, pp. 264–270.

[13] Blelloch, P. A., and Carney, K. S., "Modal Representations in Control/Structure Interaction," *Proceedings of the American Control Conference* (Pittsburgh, PA), Inst. of Electrical and Electronics Engineers, 1989, pp. 2802–2807.

[14] Balas, M., "Feedback Control of Flexible Systems," *IEEE Transactions on Automatic Control*, Vol. 23, 1978, pp. 673–679.

[15] Balas, M. J., "Low-Order Control of Linear Finite Element Models of Large Flexible Space Structures Using Second-Order Parallel Architecture," *Mechanics and Control of Large Flexible Structures*, edited by J. L. Junkins, Vol. 129, Progress in Astronautics and Aeronautics, AIAA, Washington, DC, 1990, pp. 295–313.